Femtosecond x-ray diffraction study of multi-THz coherent phonons in SrTiO$_3$

Roman Shayduk, Jörg Hallmann, Angel Rodriguez-Fernandez, et al.

ARTICLES YOU MAY BE INTERESTED IN

Femtosecond x-ray diffraction study of multi-THz coherent phonons in SrTiO₃

Roman Shayduk,[1,a] [iD] Jörg Hallmann,[1] Angel Rodriguez-Fernandez,[1] Markus Scholz,[1,2] Wei Lu,[1] Ulrike Bösenberg,[1] Johannes Möller,[1] Alexey Zozulya,[1] Man Jiang,[1] Ulrike Wegner,[1] Radu-Costin Secareanu,[1] Guido Palmer,[1] Moritz Emons,[1] Max Lederer,[1] Sergey Volkov,[2] Ionela Lindfors-Vrejoiu,[3] [iD] Daniel Schick,[4] [iD] Marc Herzog,[5] [iD] Matias Bargheer,[5] [iD] and Anders Madsen[1] [iD]

AFFILIATIONS

[1]European X-Ray Free-Electron Laser Facility GmbH, Holzkoppel 4, 22869 Schenefeld, Germany
[2]Deutsches Elektronen-Synchrotron DESY, Notkestraße 85, 22607 Hamburg, Germany
[3]University of Cologne, Institute of Physics II, Zülpicher Str. 77, 50937 Cologne, Germany
[4]Max-Born-Institut (MBI) im Forschungsverbund Berlin e.V., Max-Born-Straße 2A, 12489 Berlin, Germany
[5]Universität Potsdam, Institut für Physik and Astronomie, Campus Golm, Haus 28, Karl-Liebknecht-Straße 24/25, 14476 Potsdam-Golm, Germany

[a]Author to whom correspondence should be addressed: roman.shayduk@xfel.eu

ABSTRACT

We report generation of ultra-broadband longitudinal acoustic coherent phonon wavepackets in SrTiO₃ (STO) with frequency components extending throughout the first Brillouin zone. The wavepackets are efficiently generated in STO using femtosecond infrared laser excitation of an atomically flat 1.6 nm-thick epitaxial SrRuO₃ film. We use femtosecond x-ray diffraction at the European X-Ray Free Electron Laser Facility to study the dispersion and damping of phonon wavepackets. The experimentally determined damping constants for multi-THz frequency phonons compare favorably to the extrapolation of a simple ultrasound damping model over several orders of magnitude.

Acoustic phonons play an important role in heat transport phenomena. At room temperature, the transport of heat in dielectrics is accomplished by the diffusion of acoustic phonons determined by three-phonon interactions.[1] Scattering of high frequency acoustic phonons due to the Umklapp process limits the heat flow.[2] There are various mechanisms of phonon scattering (e.g., Akhiezer, Landau-Rumer, and Herring processes). Although a crossover from low- to high-frequency phonons is expected,[3–5] typically the phonon damping rate has a dominant proportionality to the squared frequency ($\propto \omega^2$) or squared wavevector ($\propto k^2$) in the linear region of the phonon dispersion. Both inelastic neutron- and x-ray scattering can provide full dispersion relations,[6] and recently, thermal diffuse scattering in a pump-probe configuration has become available to assess dynamic changes of phonon populations, even on ultrashort timescales after laser-heating.[7,8] Determining the imaginary part of the dispersion, i.e., the linewidth, is often a challenge due to the finite instrument resolution function. Ultrafast x-ray scattering from coherent phonons is a method that has extended the picosecond-ultrasound experiments

with all optical pulses to higher wavevectors.[8–10] In particular, in SrRuO₃/SrTiO₃ (SRO/STO) heterostructures[11] and superlattices[10] with their perfect acoustic impedance matching, femtosecond laser excitation of the metallic opto-acoustic transducer was used to decouple the excitation from the detection process of coherent phonons via ultrafast x-ray diffraction (UXRD). Recent progress in four-wave-mixing (4WM) in the soft[12,13] and hard[14] x-ray range is aiming at studying phonon diffusion and, hence, accessing the damping. Such time-domain experiments can measure even very small damping from the decay of intensity oscillations as in, for example, time-domain Brillouin scattering (TDBS).[15] By following the propagating coherent wavepackets, nonlinear mixing processes, such as sum-frequency generation[16] and self-steepening[15] of phonon wavepackets, have been observed that add another coordinate in the coherent phonons' energy flow landscape. In the optical range, TDBS can be interpreted classically as an interference of the probe light reflected from the propagating sound wave with reflection from the surface.[17,18] This interpretation becomes invalid for wavepackets extending to the first

Brillouin-zone (BZ) boundary, where the group velocity is zero. However, describing the same process as inelastic scatting of photons (visible light or x rays) can be applied throughout the BZ.[9,18]

Understanding of the generation, propagation, and interaction of high-wavevector coherent phonons is especially important in materials exhibiting photoinduced phase transitions[19,20] and for designing heterostructures for future nano-opto-electronics with the desired length scale approaching a few atomic unit cells. The metallic oxide $SrRuO_3$ and the insulating oxide $SrTiO_3$ are extremely robust under strong optical excitation.[15] The phonon damping constant Γ and anomalies of the sound velocity v of STO have been widely discussed in the context of the ferro-distortive phase transition at $T = 105$ K.[21,22] Results from conventional MHz ultrasound experiments and TDBS in the GHz range and up to 1 THz have confirmed the quadratic dependence of the damping constant on the wavevector.[22–24]

In this Letter, we report the excitation and observation of broadband longitudinal acoustic coherent phonons in single crystalline STO with frequency components covering the entire Brillouin zone. Upon femtosecond IR laser excitation with a fluence of approximately 10 mJ/cm² of an atomically flat 1.6 nm-thick epitaxial SRO transducer film, we observe a wavepacket that contains frequency components up to 4.5 THz. The wavepacket propagates at a strongly reduced group velocity of less than half of the longitudinal sound velocity. Intriguingly, the damping of these high frequency components is still consistent with an extrapolation of ultrasound measurements over several orders of magnitude.

The ultrafast pump-probe experiment was carried out at the materials imaging and dynamics (MID) station of the European X-ray Free-Electron Laser Facility (XFEL)[25] (see "Experimental details" in the supplementary material).

The atomically flat SRO opto-acoustic transducer and SRO/STO interface are key to the observation of wavevector components near the Brillouin zone boundary. It was grown on a vicinal STO (001) single crystalline substrate using pulsed laser deposition (PLD).[26] Figure 1(a) illustrates the cubic unit cell of the STO lattice. The STO surface is homogeneously covered by the SRO film with a nominal thickness of four unit cells ($d = 1.6$ nm). The surface topography map [Fig. 1(b)] of the sample used in the experiment measured by atomic force microscopy (AFM) exhibits a root mean square surface roughness of 0.4 nm, corresponding to one unit cell. It is well known that the step-flow growth results in terraces with approximately 200 nm width and a one unit cell step height.[26–28] Figure 1(c) shows a specular x-ray reflectivity curve of the sample as a function of the reciprocal lattice coordinate L (continuous value of the Miller index). In the specular scattering geometry, the x-ray wavevector transfer is given by

$$q = 2k \sin \theta = L \frac{2\pi}{a},\tag{1}$$

where k is the x-ray wavevector magnitude, θ is the x-ray incidence angle with respect to the Bragg planes, and a is the STO lattice constant of 3.905 Å. For integer L, Eq. (1) is equivalent to Bragg's law. The green dots in Fig. 1(c) show reflectivity data obtained at the high-resolution synchrotron beamline P08 (DESY) operated at 9 keV.[29] Solid lines represent the simulated x-ray reflectivity for two perfectly flat representations of a bare STO substrate (blue) and a four-unit cell-thick SRO layer on STO (orange). The surface and interface roughness of the sample suppresses the scattering far away from Bragg positions
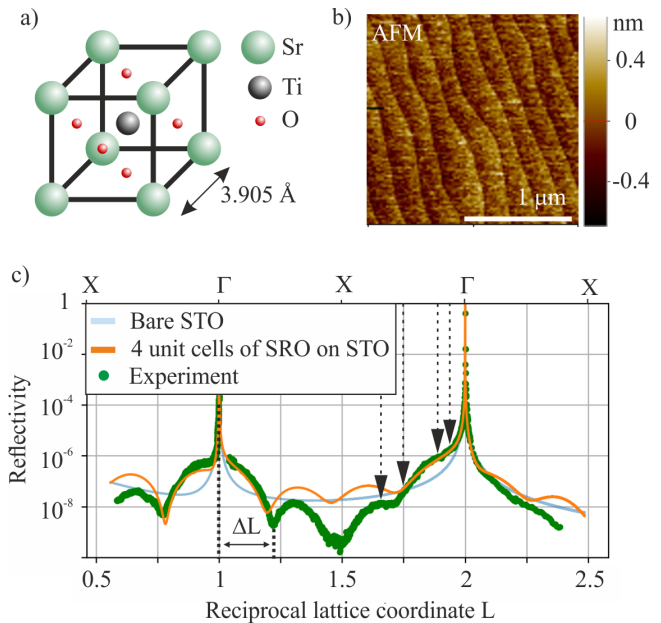

FIG. 1. (a) Cubic unit cell of $SrTiO_3$ with a perovskite structure. (b) Atomic force microscopy topograph of the $SrRuO_3$ thin film grown on the STO crystal. (c) Plot of extended x-ray reflectivity curves along the specular (001) direction. Green dots indicate experimental data collected for the sample at P08 (DESY). Calculations by dynamical x-ray diffraction for a bare, semi-infinite TiO_2-terminated single crystal of STO (blue) and for an SRO/STO heterostructure with a four unit cell thick SRO film (orange) are shown for comparison. The upper x-axis shows Γ and X as the STO Brillouin zone center and boundary, respectively. Dashed vertical arrows indicate positions at which time series in Fig. 2 were taken.

and explains the deviations between the simple model and the data. The out-of-plane lattice constant 3.95 Å of epitaxially strained SRO on STO is slightly larger than the bulk value of 3.93 Å due to the Poisson effect.[30]

The thickness of the SRO film is determined from the period of Kiessig fringes;[31] the observed fringe period ΔL is related to the thickness as $\Delta L = \frac{1}{N}$, where $N = 4$ is the thickness of the film in unit cells, as evident from Fig. 1(c).

Figure 2 illustrates the specularly scattered x-ray intensity change as a function of the pump-probe delay for four different values of the reciprocal space coordinate indicated by vertical dashed arrows in Fig. 1(c). The intensity was integrated over a small region of the detector corresponding to the given momentum transfer. The experimental points were normalized by the values of the integrated intensity obtained at negative pump-probe delays after subtraction of a background signal (see "Data acquisition and reduction" in the supplementary material).

The measured signal is the result of interference between x rays scattered from the semi-infinite STO substrate and the SRO thin film with a very broad maximum at $L = 2 \times \frac{3.905}{3.95} = 1.98$ given by the relative out-of-plane lattice constants of STO and SRO. Qualitatively, the transient scattering signal is caused by the shift of the broad SRO Bragg peak and changes of the Kiessig fringes, which originate from the ultrafast expansion of the SRO film.[32] The expansion shifts the broad maximum of the thin film scattering from $L = 1.98$ toward
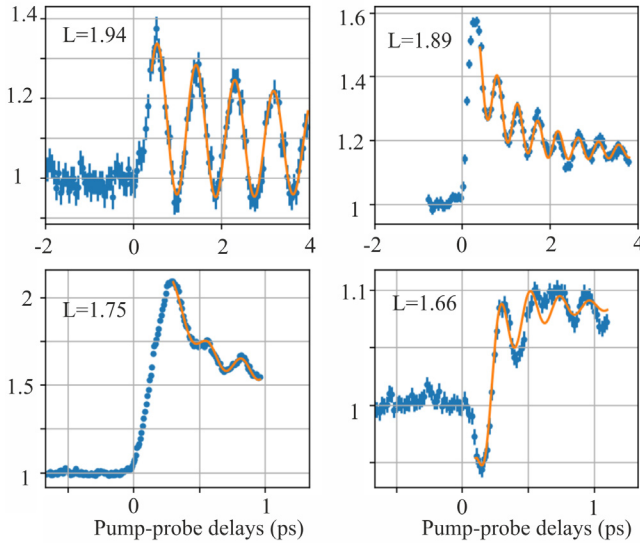
FIG. 2. Blue dots indicate experimental data points for self-normalized time-dependent specular x-ray intensity after laser excitation obtained at different reciprocal lattice coordinates L (see "Data acquisition and reduction" of the supplementary material). Error bars denote systematic errors equal to the standard deviation (2σ) of the signal measured at negative pump-probe delays. Orange line plots the fitting function according to Eq. (2) using the parameters listed in Table I.

lower values. This causes the rapid rise [or fall, depending on the probed reciprocal lattice coordinate, see Fig. 1(c)] of the scattered intensity on the femtosecond time scales and a slower decay on the ps timescale, as the SRO film is dissipating energy into the STO substrate via coherent and incoherent phonon transport.

The central results of the experiment are the pump-probe signal oscillations in the THz range, which originate from the scattering of x rays by the propagating acoustic phonon wavepacket. We can rationalize the dependence of the frequency on the probed reciprocal space coordinate L in the following way: The detected oscillatory x-ray intensity is caused by the interference of x-ray photons that are elastically scattered (from the SRO film and the undisturbed fraction of the STO substrate) with the inelastically scattered x rays by coherent phonons with wavevector k_{ph}. This interference oscillates with angular frequency $\omega(k_{ph})$, thus encoding the dispersion relation of the acoustic phonons. The specular diffraction geometry makes the experiment exclusively sensitive to longitudinal polarization components.

TABLE I. Best fit parameters.

L	1.94	1.89	1.75	1.66
A0	1.07 ± 0.02	1.16 ± 0.01	1.57 ± 0.01	1.09 ± 0.01
A1	0.11 ± 0.01	0.44 ± 0.01	2.00 ± 0.04	0.44 ± 0.01
A2	0.20 ± 0.01	0.14 ± 0.01	0.05 ± 0.01	0.06 ± 0.01
τ_1 (ps)	1.73 ± 0.80	0.75 ± 0.01	0.21 ± 0.01	0.75 ± 0.01
τ_2 (ps)	7.73 ± 1.30	1.90 ± 0.04	∞ (fixed)	0.43 ± 0.02
ν (THz)	1.13 ± 0.01	2.17 ± 0.01	3.97 ± 0.01	4.59 ± 0.05
ϕ	4.00 ± 0.05	3.26 ± 0.02	0.00 ± 0.04	5.47 ± 0.05

In order to extract the oscillation frequencies, we introduce a universal fitting function for the four measured time series

$$s(t) = A_0 + A_1 e^{-\frac{t}{\tau_1}} + A_2 e^{-\frac{t}{\tau_2}} \sin(2\pi\nu t + \phi), \qquad (2)$$

where A_0, A_1, A_2, τ_1, τ_2, ν, and ϕ are the fitting parameters. The first two terms in Eq. (2) describe the signal contribution from the SRO film. The third term is attributed to the x-ray scattering contribution from the developing coherent lattice dynamics in the STO substrate. The best fit parameters leading to the orange curves in Fig. 2 are summarized in Table I. By this analysis, we ignore the nonlinear processes of self-steepening wavepackets discussed previously for lower frequencies.[15]

We now interpret the intensity oscillations as resulting from the scattering of x rays from coherent acoustic phonons in STO with wavevector k_{ph} according to the modified Laue equation[18]

$$\boldsymbol{k}_s - \boldsymbol{k}_i = \boldsymbol{G}_{\mathrm{Br}} \pm \boldsymbol{k}_{ph}, \qquad (3)$$

in which $\boldsymbol{k}_{i/s}$ is the wavevector of incident/scattered x rays and $\boldsymbol{G}_{\mathrm{Br}}$ is a reciprocal lattice vector. As indicated above, in the current study, we use $\boldsymbol{G}_{\mathrm{Br}} = (002)$ in reciprocal lattice units.

The longitudinal acoustic phonon (LAP) wavevector in each of the experimental time series shown in Fig. 2 is

$$k_{ph} = \frac{2\pi}{a}(2 - L). \qquad (4)$$

In Fig. 3, the fitting parameter $\nu = \omega/2\pi$ is identified as the phonon frequency and plotted (red squares) as a function of k_{ph}. The results show excellent agreement with inelastic neutron scattering data[6] for the LAP dispersion of SrTiO$_3$ (black circles). The blue solid line indicates the sound velocity of STO $v = \frac{\omega}{k_{ph}} = 7.7$ km/s, and the black dotted line indicates the considerably lower group velocity $v = \frac{d\omega}{dk_{ph}} = 2.7$ km/s, extracted from the two measurements at
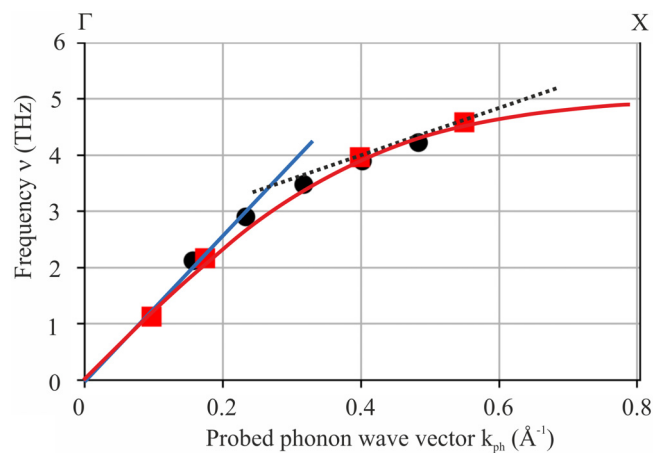

FIG. 3. Black circles indicate inelastic neutron scattering data,[6] and red squares indicate oscillation frequencies obtained in this experiment. The blue line represents the linear part of the dispersion with a longitudinal acoustic sound velocity of 7.8 km/s. The black dotted line shows the considerably lower group velocity of the high frequency components in the experiment. The red curve reproduces the LA phonon dispersion curve for STO calculated from first principles.[33] The horizontal axis range is chosen to fit the ΓX line of the STO Brillouin zone.

wavevectors at approximately 2/3 of the BZ edge. The red solid line reproduces a calculated LAP dispersion relation.[33]

In Fig. 4, we plot the damping constant $\Gamma = 1/\tau_2$ of the observed phonon oscillations as a function of the wavevector together with literature data from ultrasound measurements,[23] frequency and time-domain Brillouin scattering,[22,34] photoelastic detection (PE),[24] and previous UXRD experiments.[10,22] Clearly, the damping is proportional to k_{ph}^2 over many orders of magnitude, which is consistent with Akhiezer's theory of relaxation damping.[35] The striking result of the current study is the fact that the damping rates seem to essentially follow the k_{ph}^2-law almost all the way to the Brillouin zone boundary, although according to Akhiezer's theory the damping rate is actually expected to saturate at high frequencies.[3,5] Other mechanisms like Herring processes are believed to dominate the damping at such high frequencies and also yield a squared frequency dependence; however, the corresponding damping rate should be a few orders of magnitude lower.[3,5] The observed high damping rates may be the manifestation of nonlinear coherent phonon conversion effects[10,11,15] due to the large-amplitude atomic displacements in the generated coherent LAP wavepackets. This scenario is further supported by the fact that the high-frequency oscillations in Fig. 2 at L = 1.66 seem to exhibit a beating instead of a simple exponentially decaying envelope function,[15] as evidenced by the poor fit quality. Further fluence-dependent studies are necessary to elucidate this question.

In conclusion, we have shown that ultrafast x-ray scattering provides a wavevector-selective probe of the frequency and damping of coherent longitudinal acoustic phonons across the entire Brillouin zone. The complex-valued dispersion relation that represents propagation and damping of phonons can be directly extracted from the scattering angle and the observed intensity oscillations. The generation of wavevector components reaching out to the BZ boundary of $SrTiO_3$ is enabled by the monatomic flatness of the surface and the interface of the ultrathin $SrRuO_3$ film, which absorbs the pump light. The observed frequencies are in accordance with earlier inelastic neutron scattering data[6] and phonon dispersion calculations from first principles.[33] The observed damping is in good accordance with a k^2 law extrapolating from measurements at much smaller k. In addition to the possibility of investigating the fundamental damping mechanisms at very large wavevectors, such experiments pave the road to the direct observation of previously inaccessible nonlinear phonon-mixing processes that involve large-wavevector acoustic phonons relevant for Umklapp-processes that limit thermal transport in condensed matter.

See the supplementary material for "Experimental details" section for the technical details of the pump-probe x-ray diffraction experiment. For details on the data collection and normalization presented in Fig. 2, see "Data acquisition and reduction" section.

AUTHOR DECLARATIONS
Conflict of Interest

The authors have no conflicts to disclose.

DATA AVAILABILITY

The data that support the findings of this study are available from the corresponding author upon reasonable request.
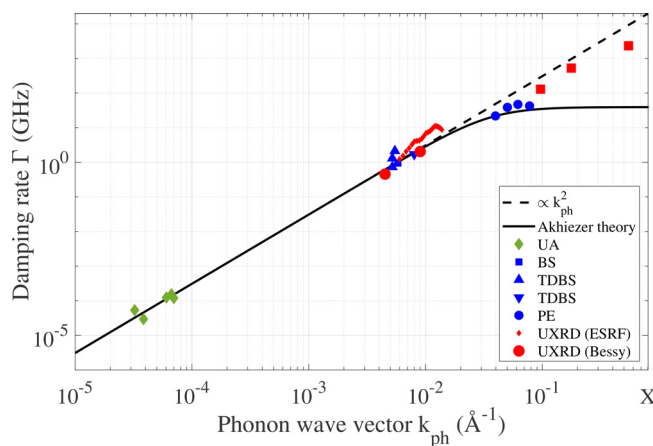

FIG. 4. Collection of experimental acoustic damping constants in STO from ultrasonic attenuation (UA),[23] Brillouin scattering in the frequency domain (BS) and time domain (TDBS),[22,34] photoelastic detection (PE),[24] sub-ns,[10,22] and sub-ps x-ray scattering presented in this study (red solid squares). The solid black line reproduces the predictions of Akhiezer's relaxation theory along with an extrapolation of the k_{ph}^2-law (dashed black line). Note that the abscissa extends until the Brillouin zone boundary.

REFERENCES

[1]L. Lindsay, C. Hua, X. Ruan, and S. Lee, "Survey of *ab initio* phonon thermal transport," Mater. Today Phys. **7**, 106–120 (2018).

[2]N. W. Ashcroft and N. D. Mermin, *Solid State Physics* (Saunders College Publishing, 1976).

[3]B. C. Daly, "Picosecond ultrasonic measurements of attenuation of longitudinal acoustic phonons in silicon," Phys. Rev. B **80**, 174112 (2009).

[4]W. Chen, H. J. Maris, Z. R. Wasilewski, and S.-I. Tamura, "Attenuation and velocity of 56 GHz longitudinal phonons in gallium arsenide from 50 to 300 k," Philos. Mag. B **70**, 687–698 (1994).

[5]A. Maznev, F. Hofmann, A. Jandl, K. Esfarjani, M. T. Bulsara, E. A. Fitzgerald, G. Chen, and K. A. Nelson, "Lifetime of sub-THz coherent acoustic phonons in a GaAs-AlAs superlattice," Appl. Phys. Lett. **102**, 041901 (2013).

[6]R. A. Cowley, "Lattice dynamics and phase transitions of strontium titanate," Phys. Rev. **134**, A981–A997 (1964).

[7]M. Trigo, J. Chen, V. H. Vishwanath, Y. M. Sheu, T. Graber, R. Henning, and D. A. Reis, "Imaging nonequilibrium atomic vibrations with x-ray diffuse scattering," Phys. Rev. B **82**, 235205 (2010).

[8]M. Trigo, M. Fuchs, J. Chen, M. P. Jiang, M. Cammarata, S. Fahy, D. M. Fritz, K. Gaffney, S. Ghimire, A. Higginbotham, S. L. Johnson, M. E. Kozina, J. Larsson, H. Lemke, A. M. Lindenberg, G. Ndabashimiye, F. Quirin, K. Sokolowski-Tinten, C. Uher, G. Wang, J. S. Wark, D. Zhu, and D. A. Reis, "Fourier-transform inelastic x-ray scattering from time- and momentum-dependent phonon–phonon correlations," Nat. Phys. **9**, 790–794 (2013).

[9]T. Henighan, M. Trigo, S. Bonetti, P. Granitzka, D. Higley, Z. Chen, M. P. Jiang, R. Kukreja, A. Gray, A. H. Reid, E. Jal, M. C. Hoffmann, M. Kozina, S. Song, M. Chollet, D. Zhu, P. F. Xu, J. Jeong, K. Carva, P. Maldonado, P. M. Oppeneer, M. G. Samant, S. S. P. Parkin, D. A. Reis, and H. A. Dürr,

"Generation mechanism of terahertz coherent acoustic phonons in Fe," Phys. Rev. B **93**, 220301 (2016).

[10] R. Shayduk, M. Herzog, A. Bojahr, D. Schick, P. Gaal, W. Leitenberger, H. Navirian, M. Sander, J. Goldshteyn, I. Vrejoiu, and M. Bargheer, "Direct time-domain sampling of subterahertz coherent acoustic phonon spectra in SrTiO₃ using ultrafast x-ray diffraction," Phys. Rev. B **87**, 184301 (2013).

[11] M. Herzog, A. Bojahr, J. Goldshteyn, W. Leitenberger, I. Vrejoiu, D. Khakhulin, M. Wulff, R. Shayduk, P. Gaal, and M. Bargheer, "Detecting optically synthesized quasimonochromatic sub-terahertz phonon wavepackets by ultrafast x-ray diffraction," Appl. Phys. Lett. **100**, 094101 (2012).

[12] F. Bencivenga, R. Cucini, F. Capotondi, A. Battistoni, R. Mincigrucci, E. Giangrisostomi, A. Gessini, M. Manfredda, I. P. Nikolov, E. Pedersoli, E. Principi, C. Svetina, P. Parisse, F. Casolari, M. B. Danailov, M. Kiskinova, and C. Masciovecchio, "Four-wave mixing experiments with extreme ultraviolet transient gratings," Nature **520**, 205 (2015).

[13] F. Bencivenga, R. Mincigrucci, F. Capotondi, L. Foglia, D. Naumenko, A. A. Maznev, E. Pedersoli, A. Simoncig, F. Caporaletti, V. Chiloyan, R. Cucini, F. Dallari, R. A. Duncan, T. D. Frazer, G. Gaio, A. Gessini, L. Giannessi, S. Huberman, H. Kapteyn, J. Knobloch, G. Kurdi, N. Mahne, M. Manfredda, A. Martinelli, M. Murnane, E. Principi, L. Raimondi, S. Spampinati, C. Spezzani, M. Trovò, M. Zangrando, G. Chen, G. Monaco, K. A. Nelson, and C. Masciovecchio, "Nanoscale transient gratings excited and probed by extreme ultraviolet femtosecond pulses," Sci. Adv. **5**, eaaw5805 (2019).

[14] J. R. Rouxel, D. Fainozzi, R. Mankowsky, B. Rosner, G. Seniutinas, R. Mincigrucci, S. Catalini, L. Foglia, R. Cucini, F. Doring, A. Kubec, F. Koch, F. Bencivenga, A. Al Haddad, A. Gessini, A. A. Maznev, C. Cirelli, S. Gerber, B. Pedrini, G. F. Mancini, E. Razzoli, M. Burian, H. Ueda, G. Pamfilidis, E. Ferrari, Y. Deng, A. Mozzanica, P. J. M. Johnson, D. Ozerov, M. G. Izzo, C. Bottari, C. Arrell, E. J. Divall, S. Zerdane, M. Sander, G. Knopp, P. Beaud, H. T. Lemke, C. J. Milne, C. David, R. Torre, M. Chergui, K. A. Nelson, C. Masciovecchio, U. Staub, L. Patthey, and C. Svetina, "Hard x-ray transient grating spectroscopy on bismuth germanate," Nat. Photonics **15**, 499 (2021).

[15] A. Bojahr, M. Herzog, D. Schick, I. Vrejoiu, and M. Bargheer, "Calibrated real-time detection of nonlinearly propagating strain waves," Phys. Rev. B **86**, 144306 (2012).

[16] A. Bojahr, M. Gohlke, W. Leitenberger, J. Pudell, M. Reinhardt, A. von Reppert, M. Roessle, M. Sander, P. Gaal, and M. Bargheer, "Second harmonic generation of nanoscale phonon wave packets," Phys. Rev. Lett. **115**, 195502 (2015).

[17] C. Thomsen, H. T. Grahn, H. J. Maris, and J. Tauc, "Surface generation and detection of phonons by picosecond light pulses," Phys. Rev. B **34**, 4129–4138 (1986).

[18] A. Bojahr, M. Herzog, S. Mitzscherling, L. Maerten, D. Schick, J. Goldshteyn, W. Leitenberger, R. Shayduk, P. Gaal, and M. Bargheer, "Brillouin scattering of visible and hard x-ray photons from optically synthesized phonon wave-packets," Opt. Express **21**, 21188–21197 (2013).

[19] O. Y. Gorobtsov, L. Ponet, S. K. K. Patel, N. Hua, A. G. Shabalin, S. Hrkac, J. Wingert, D. Cela, J. M. Glownia, D. Zhu, R. Medapalli, M. Chollet, E. E. Fullerton, S. Artyukhin, O. G. Shpyrko, and A. Singer, "Femtosecond control of phonon dynamics near a magnetic order critical point," Nat. Commun. **12**, 2865 (2021).

[20] S. O. Mariager, F. Pressacco, G. Ingold, A. Caviezel, E. Moehr-Vorobeva, P. Beaud, S. L. Johnson, C. J. Milne, E. Mancini, S. Moyerman, E. E. Fullerton, R. Feidenhans'l, C. H. Back, and C. Quitmann, "Structural and magnetic dynamics of a laser induced phase transition in FeRh," Phys. Rev. Lett. **108**, 087201 (2012).

[21] L. Maerten, A. Bojahr, M. Gohlke, M. Rössle, and M. Bargheer, "Coupling of GHz phonons to ferroelastic domain walls in SrTiO₃," Phys. Rev. Lett. **114**, 047401 (2015).

[22] L. Maerten, A. Bojahr, M. Reinhardt, A. Koreeda, M. Rössle, and M. Bargheer, "Critical behavior of the damping rate of GHz acoustic phonons in SrTiO₃ at the antiferrodistortive phase transition measured by time- and frequency-resolved Brillouin scattering," arXiv:1810.00381 (2018).

[23] R. Nava, R. Callarotti, H. Ceva, and A. Martinet, "Hypersonic attenuation by low-frequency optical phonons in SrTiO₃ crystals," Phys. Rev. **188**, 1456–1464 (1969).

[24] C.-Y. Yang, P.-C. Wu, Y.-H. Chu, and K.-H. Lin, "Generation and coherent control of terahertz acoustic phonons in superlattices of perovskite oxides," New J. Phys. **23**, 053009 (2021).

[25] A. Madsen, J. Hallmann, G. Ansaldi, T. Roth, W. Lu, C. Kim, U. Boesenberg, A. Zozulya, J. Möller, R. Shayduk, M. Scholz, A. Bartmann, A. Schmidt, I. Lobato, K. Sukharnikov, M. Reiser, K. Kazarian, and I. Petrov, "Materials Imaging and Dynamics (MID) instrument at the European X-ray Free-Electron Laser Facility," J. Synchrotron Radiat. **28**, 637–649 (2021).

[26] F. Bern, M. Ziese, A. Setzer, E. Pippel, D. Hesse, and I. Vrejoiu, "Structural, magnetic and electrical properties of SrRuO₃ films and SrRuO₃/SrTiO₃ super-lattices," J. Phys.: Condens. Matter **25**, 496003 (2013).

[27] J. Choi, C. Eom, G. Rijnders, H. Rogalla, and D. Blank, "Growth mode transition from layer by layer to step flow during the growth of heteroepitaxial SrRuO₃ on (001) SrTiO₃," Appl. Phys. Lett. **79**, 1447–1449 (2001).

[28] M. Ziese, I. Vrejoiu, and D. Hesse, "Structural symmetry and magnetocrystalline anisotropy of SrRuO₃ films on SrTiO₃," Phys. Rev. B **81**, 184418 (2010).

[29] O. H. Seeck, C. Deiter, K. Pflaum, F. Bertam, A. Beerlink, H. Franz, J. Horbach, H. Schulte-Schrepping, B. M. Murphy, M. Greve, and O. Magnussen, "The high-resolution diffraction beamline P08 at PETRA III," J. Synchrotron Radiat. **19**, 30–38 (2012).

[30] M. Herzog, W. Leitenberger, R. Shayduk, R. M. van der Veen, C. J. Milne, S. L. Johnson, I. Vrejoiu, M. Alexe, D. Hesse, and M. Bargheer, "Ultrafast manipulation of hard x-rays by efficient Bragg switches," Appl. Phys. Lett. **96**, 161906 (2010).

[31] B. E. Warren, *X-Ray Diffraction* (Dover Publications, Inc, New York, 1990).

[32] D. Schick, A. Bojahr, M. Herzog, R. Shayduk, C. von Korff Schmising, and M. Bargheer, "Udkm1Dsim—A simulation toolkit for 1D ultrafast dynamics in condensed matter," Comput. Phys. Commun. **185**, 651–660 (2014).

[33] L. Feng, T. Shiga, and J. Shiomi, "Phonon transport in perovskite SrTiO₃ from first principles," Appl. Phys. Express **8**, 071501 (2015).

[34] A. Nagakubo, A. Yamamoto, K. Tanigaki, H. Ogi, N. Nakamura, and M. Hirao, "Monitoring of longitudinal-wave velocity and attenuation of SrTiO₃ at low temperatures using picosecond ultrasound spectroscopy," Jpn. J. Appl. Phys. **51**, 07GA09 (2012).

[35] H. J. Maris, "Interaction of sound waves with thermal phonons in dielectric crystals," in *Physical Acoustics* (Academic Press, Inc., 1971), Vol. 8, pp. 279–345.